Plasmon Near-Field Coupling in Metal Dimers as a Step toward Single-Molecule Sensing

Srdjan S. Aćimović,[†] Mark P. Kreuzer,[†] María U. González,[†] and Romain Quidant[†,‡,*]

[†]ICFO-Institut de Ciencies Fotoniques, Mediterranean Technology Park, Castelldefels, Barcelona, 08860 Spain, and [‡]Institució Catalana de Recerca i Estudis Avançats (ICREA), Barcelona, 08010 Spain

ABSTRACT In this study, we report on ultrasensitive protein detection with lithographically prepared plasmonic nanostructures. We have engineered optical nanosensors by the combined approach of negative resist, electron beam lithography, and reactive ion etching to form highly reproducible arrays of gold dimers in which the near-field coupling in their subwavelength gap enables for scaling the sensing volume down to the single-protein scale. In good agreement with recent theoretical predictions, the dimer geometry offers enhanced sensitivity compared to isolated particles for the detection of both small organic molecules and proteins. Beyond, by exploiting size exclusion, we are capable of monitoring the number of proteins able to bind across the gap region through the precise engineering of the structures coupled to the selective binding of a surface-assembled monolayer and covalent attachment of the protein.

KEYWORDS: localized surface plasmon · near-field coupling · gold dimers · e-beam lithography · small organic molecule · protein detection

Localized surface plasmon (LSP) resonances supported by noble metal nanostructures (MNs) have recently stimulated extensive efforts motivated by ultrasensitive biochemical optical detection.[1−4] Beyond using enhanced plasmon fields to increase the Raman scattering cross section in surface-enhanced Raman scattering (SERS) experiments,[5,6] one can take advantage of the intrinsic sensitivity of LSP resonances to small changes of the shallow refraction index at the metal surface to use MNs as efficient and compact colorimetric sensors.[7] While LSP sensor performance is not expected to compete with surface plasmon polariton systems, based on flat metal films (SPR) in detecting bulk refractive index changes, they are more likely to enable a higher sensitivity to local perturbations such as those induced by small molecule binding events occurring at the metal surface. The main advantage of resonant MNs over metal films relies on the possibility for an accurate engineering of their optical properties by controlling and changing their size, shape, composition, and environment.[8] In practice, the sensitivity of LSP sensors is determined by both the spectral features of the plasmon resonance and the spatial distribution of the associated mode. On the one hand, the accuracy in resolving a tiny frequency shift of the LSP resonance is determined by the ratio between the magnitude of the shift and the resonance bandwidth. While the absorption of metals in the optical range is responsible for rather broad resonances, several works have lately pointed out configurations of coupled MNs which enable the achievement of sharp spectral features.[9,10] On the other hand, the magnitude of the shift is itself defined by the perturbation induced by the local change of refraction index to the mode volume. It is now well-known that the electromagnetic coupling between adjacent MNs can lead to a subwavelength confinement of light. In particular, strong field confinement can be achieved in the subwavelength gap between closely spaced MNs when the incident field has a component driving the metal surface charges across the gap.[11−14] While the so-called plasmonic dimers (also known as gap antennas) are good candidates for SERS applications,[15] it has been suggested that they could as well substantially benefit to improve the sensitivity of LSP sensing over isolated MNs when applied to very local changes of the refraction index as induced by the presence of few or single molecules.[16,17] However, there exist few techniques capable of engineering gap dimers with high precision and control and thus far this type of sensing has been unachievable. In addition, most sensing platforms to date lack sensitivity and necessitate the use of labels to monitor or visualize the binding event of small

*Address correspondence to romain.quidant@icfo.es.

Received for review February 2, 2009 and accepted April 14, 2009.

Published online April 22, 2009.
10.1021/nn900102j CCC: $40.75

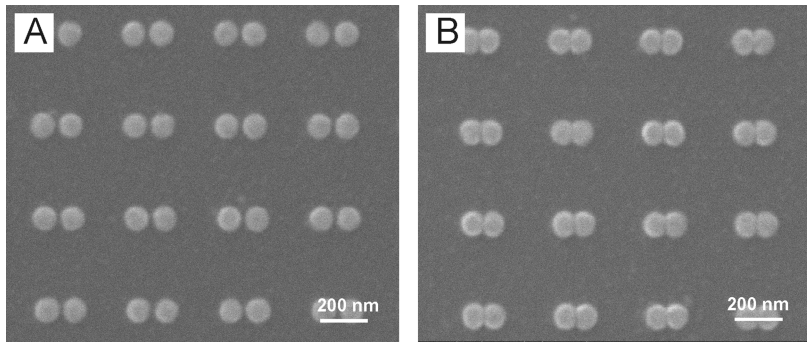

Figure 1. SEM micrographs of patterned arrays of separated dimers (a) and overlapping particles (b) obtained by the combination of negative resist e-beam lithography and RIE.

molecular weight analytes. Label-less sensing has thus been limited to larger analyte molecules in the few thousand Dalton range (or higher). Herein, we present the systematic development of such bio(chemical) sensors through the amalgamation of nanoscale fabrication, optical characterization, chemical modification, and biological binding of the target in what we believe to be the first experimental demonstration of enhanced sensitivity of protein detection with plasmonic dimers. Beyond confirming prior theoretical predictions, our data reveals the potential of this approach to discriminate the number of protein molecules able to physically fit across the dimers nanogap, opening new perspectives toward further specificity based on size exclusion.

RESULTS AND DISCUSSION

There currently exists high interest in the detection of low concentration of proteins and/or small molecules (diagnostic proteomics) motivated by key applications to biomedicine, food assessment, and doping control. While both chemically synthesized metal colloids and lithographically prepared metal nanostructures have been used as biochemical sensors based on a shift of their LSP resonance, their sensitivity has not yet reached the level to compete with commercially available SPR sensing based on flat metal films. While several recent theoretical works have predicted the enhanced sensitivity of plasmon dimers, an experimental implementation is challenging mainly due to high requirements on the dimers' quality.[13,16,23] To fulfill these requirements, we have developed a fabrication protocol combining e-beam lithography and reactive ion etching which facilitates the manufacturing of highly uniform dimer arrays with consistently small gaps (<10 nm) between adjacent particles. We have subsequently utilized chemical surface assembly, activation, and cross-linking to selectively bind a protein of choice and optical extinction spectroscopy to monitor the resulting changes in the dimers' resonance. Through the geometric design and reproducible fabrication, improved detection levels are realized by these plasmonic nanosensors (dimers), sufficient to allow detection of small organic molecules and proteins when compared to existing nanostructured systems (isolated MNs). Remarkably, our configuration is sensitive enough to clearly detect whether the analyte can penetrate into the sensing volume defined by the dimer nanogap, opening new perspectives toward single-molecule sensing, size discrimination, and binding orientation studies.

Sample Preparation. A large number of prior studies on LSP sensing have focused on single colloidal MNs mainly motivated by cheap synthesis and sharper resonances associated with metal crystallinity.[18] However, besides critical issues arising from particle size dispersion, the accurate positioning of colloids onto a substrate remains challenging and, consequently, hinders the use of arrays for multiplexed sensing and controlled arrangements for increased sensitivity. Alternatively, nanosphere lithography (NSL) is a cheap and parallel process that has been extensively used to fabricate large arrays of LSP sensors able to detect amyloid-β,[19] antibiotin antibody,[20] and surface-assembled monolayer of 1-HDT with zeptomole sensitivity.[21] In order to fabricate arrays of dimers, flexibility on the shape and positioning of MNs is required and typically achieved by high-resolution scanning electron beam lithography (EBL). While standard e-beam processes based on positive electron sensitive resists such as polymethyl methacrylate (PMMA) combined with lift-off can be optimized to achieve remarkable results,[22,23] they suffer from several limitations mostly originating from the somewhat uncontrolled nature of the lift-off process, which restrict the level of reproducibility particularly when attempting to develop small gap sizes (<10 nm). In order to attain better control over the preparation of extended arrays of dimers, we have developed an alternative fabrication process combining e-beam writing on high-resolution negative resist coated on top of a Au film and reactive ion etching (RIE). This process allows us to achieve a much better level of control over crucial features, in particular, in terms of size dispersity and minimum gaps between two adjacent MNs. Furthermore, the procedure does not require the use of any additional conductive layer for charge evacuation below the metal film (indium tin oxide is usually used with positive resist) or Cr/Ti adhesion layers. As a consequence, we observe that the resulting MNs show resonances with at least 20% narrower spectral features compared to what can be achieved when these absorbing layers are introduced. Regarding adhesion, our MNs have resisted the presence of all solvents during sensing experiments as well as moderate power ultrasound bath sonication. With this fabrication process, large arrays of dimers (125 × 125 pairs) with gaps down to a few nanometers were reproducibly obtained.

Sample Characterization. In our sensing experiments, we have chosen to work with particles of 40 nm height and 100 nm in diameter. Dimers are arranged into a square lattice of 400 nm period, which is reduced to 200 nm for isolated MNs, to keep the metal density constant. Figure 1 shows scanning electron microscope (SEM) images of a portion of arrays of fused dimers and dimers separated by 25 nm.

In order to get a complete range of gap sizes, ranging from separated MNs (>100 nm) to fused dimers, during the fabrication process, we exposed several arrays (50 × 50 μm) of nanoparticle pairs with varying particle spacing. For the larger gap sizes (>40 nm), the spacing was changed by steps of 10 nm, while as structures approached touching dimers (gap <20 nm), the sampling was refined from 5 to 2 nm steps as higher detail was needed in this regime. The fabricated arrays were then probed by extinction spectroscopy in order to measure their resonance properties and to assess the gap size. Figure 2 shows the evolution of the extinction spectrum as a function of the interparticle pair separation. For fused particles, the structures behave like nanorods whose dipolar resonance (centered around 775 nm) continuously red shifts toward the near-IR as overlap decreases, and therefore, the size of this equivalent nanorod increases (Figure 2, dotted arrow). At some point, the dipolar peak shifts to the IR region (>1 μm), out of the range of our spectrometer. Further separation between the nanoparticle pairs provides even longer nanorod-shaped structures and leads to the appearance of a multipolar peak around 600 nm (Figure 2, dashed arrow), which also continually red shifts with the overlap decrease. Once the conductive bridge between the two MNs breaks, this multipolar peak evolves into the coupled dipolar mode.[13] The first instance, where the measured resonance blue shifts, for an intended 2 nm separation, is the signature of the smallest gap achievable for well-defined dimers with our fabrication process. Thereafter, the resonance exponentially blue shifts as the gap increases (Figure 2, solid arrow) and finally stabilizes around 630 nm, corresponding to an array of "isolated" MNs. The inset in Figure 2 shows the exponential evolution of the measured peak resonance corresponding to dimers as a function of the gap size, together with the least-squares fit to a single exponential function $y = y_0 + ae^{-x/l}$ with a decay length of 17.24 ± 0.8 nm and a corresponding correlation of $R^2 = 0.995$, in good agreement with previous findings.[23]

Thereafter, we also fit our experimental data to the plasmon ruler equation, $\Delta\lambda/\lambda = a \times e^{-x/\tau}$ ($\Delta\lambda$ is the resonance shift due to plasmon coupling, λ is the resonant wavelength of isolated particle, and x = gap size/particle diameter ratio), to describe the universal scaling behavior of metal dimers independently of their specific dimensions.[24,25] By plotting the plasmon shift due to particle near-field coupling, normalized to the isolated particle case, as a function to gap/diameter ratio, one expects to obtain the same parameter τ from sample to sample. In our case, τ was found to be 0.179 ± 0.016 ($R^2 = 0.989 \pm 0.011$, $N = 6$). These results agree well with, for example, 0.18 ± 0.02 recently reported[23] and further confirm our gap size estimations.

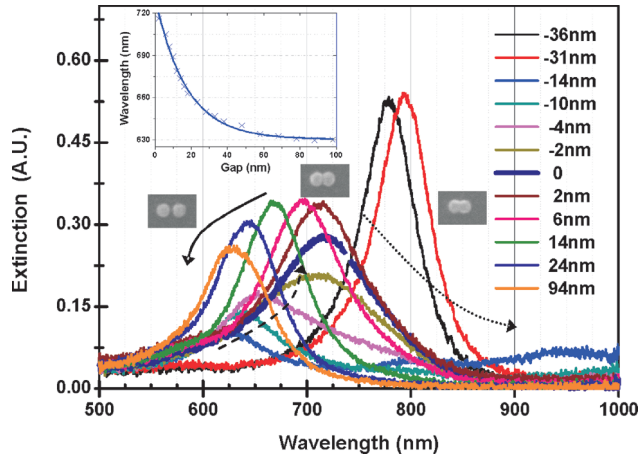

Figure 2. Evolution of the extinction spectrum from fused (negative gap values) to separated dimer arrays. Dotted arrow: Dipolar peak of overlapping MNs (high overlap) red shifts. Dashed arrow: Emergence of the multipolar resonance peaks of weakly overlapping MNs (corresponding dipolar peaks are outside of detection range in IR). Solid arrow: Blue shift of the dipolar peak of separated dimers with increasing particle separation. Inset refers to resonance peak positions as a function of gap size. The line is a least-squares fit to a single exponential function $y = y_0 + ae^{(-x/l)}$.

Sensing Experiment. Once optical characterization of the dimers was completed, sensing experiments were conducted to demonstrate the enhanced sensing ability of dimers over isolated MNs for the detection of small organic molecules and biological proteins. As part of the experimental procedure, each prepared sample is first kept in ethanol in order to rule out any changes induced by solvent. Indeed, exposure of MNs to different types of solvents can physically modify their shape and consequently affect their resonant conditions.[26] Since the most common self-assembled molecules that bind to gold are dissolved in organic solvents, one should clearly distinguish resonance shifts due to monolayer formation from structural changes provoked by the solvent (so-called solvent annealing). In a second step, the gold surface is functionalized with a self-assembled monolayer (SAM) of mercaptoundecanoic acid (MUA). MUA is a heterobifunctional alkane derivate with a 10-carbon backbone. The mercapto (thiol) headgroup is well-known to coordinate to gold surfaces by stabilizing surface atoms and modifying the electronic states. The terminal functional acid group can be easily modified and used in subsequent binding steps. Finally, after activation of the acid by carbodiimide, we bind the protein bovine serum albumin (BSA) strongly to the monolayer. After each step, the samples were optically characterized.

Figure 3a shows the resonance shifts due to solvent annealing, which will enable us to subsequently isolate

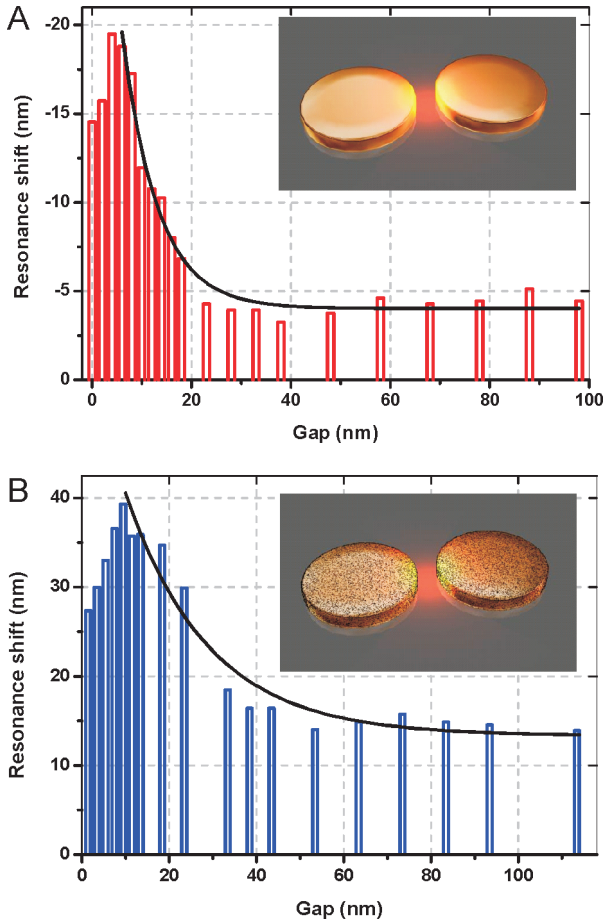

Figure 3. (a) Evolution with the gap size of the resonance blue shift (marked as negative values) induced by solvent annealing. Inset: Schematic of solvent annealed MN dimers. (b) Evolution with the gap size of the red shift induced by the SAM formation. Inset: Schematic of mercaptoundecanoic acid monolayer formation on MNs. Lines are partial exponential fit and used as a guide to the eye.

the resonance shift induced solely by the SAM formation. A change of MNs' shape during the solvent annealing process has been observed on silver NSL-made nanoparticles.[26] In this case, the main effects of the solvent, resulting from surface tension alternations after introducing particles from air to a different environment (solvent), were significant edge smoothing, in-plane diameter shrinking, and small height increase. Resonance shifts observed were substantial, ranging from a few tens of nanometers to 100 nm. In our case, the solvent annealing effect was less pronounced for the MNs' shape and fabrication process here employed observing shifts of about 5 nm for isolated or weakly coupled MNs (Figure 3a). However, these small modifications become more pronounced when MNs approach to form close dimers. In fact, resonance shifts increase exponentially with decreasing gaps and can reach up to 20−25 nm. This observation gives a first indication of the higher sensitivity of gap dimers to a small perturbation, which is in this case a slight geometrical modification. However, for smaller gap sizes, the resonance does not follow the predicted exponential trend. We perceive this as an underestimation of the overall blue shifts based on the presence of solvent traces in the gap region, leading to a partial red shift contribution.[27]

Figure 3b shows the isolated resonance shifts associated with the SAM formation. Despite the small size of MUA molecules (<1 nm), the monolayer formation is easily monitored by resonance shift. Barbillon *et al.* have recently reported and calibrated isolated metallic nanoparticle MUA sensors.[28] From calibration data for isolated gold MNs (uncoupled) shown in that work, it was seen that full monolayer coverage produces a resonance shift of *ca.* 35 nm (saturation part of the curve). Thus, by comparing our peak shifts of uncoupled MN arrays with their calibration curve, the degree of monolayer coverage can be estimated. In Figure 3b, we see a shift for isolated particles of *ca.* 15 nm, indicating 45% coverage of all MNs. Ideally, in an optimized MUA binding step, one looks for complete monolayer coverage to provide maximum available number of binding sites for the targeted analyte. A partial coverage as obtained here also works but with reduced potential. Here again, our data show an exponential increase of the resonance shifts with decreasing gap, indicating that for a given density of MUA the perturbation induced by the presence of the molecules increases as the sensing volume gets smaller. For the smallest gaps (<8 nm), the shifts no longer follow the exponential trend, similar to the plot in Figure 3a. We attribute this in part to the underestimation of the blue shift caused by solvent annealing, as mentioned above.

Using MUA as a linking molecule, we now investigate the detection of BSA protein. Contrary to the curves in Figure 3a,b, BSA binding curves are far richer

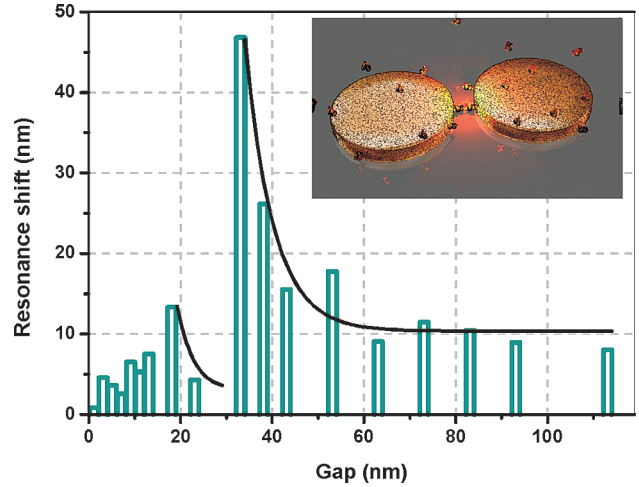

Figure 4. Evolution with the gap size of the resonance shift induced by BSA binding. Inset: Schematic of BSA protein molecule binding over SAM-modified MNs. Lines are partial exponential fit and used as a guide to the eye.

in features (Figure 4). Pertaining to previous observations, starting from isolated MNs, the red shift magnitude follows an exponential rise with decreasing separation. The maximum resonance shift is obtained when the gap reaches the size of *ca.* 30 nm.

Thereafter, as the gap further decreases, a sudden drop is observed, followed by an additional increasing trend. Again, when gap size reaches *ca.* 15 nm, another discrete drop occurs. We attribute these discrete drops to the relation between the geometry of the dimer gap and the protein size. The shape of a BSA molecule is rod-like ($4 \times 4 \times 14$ nm^3). When the gap is big enough (>30 nm), two such molecules can fit inside across the shortest distance between the dimer structure (Figure 5a). By reaching this limiting gap size of 30 nm, large resonance shifts are expected due to the optimum overlap of mode volume and BSA molecules (*ca.* 30 nm). When the gap decreases further below the first critical value, only one of the two molecules can now fit along the dimer axis, bound either to one or the other MN (Figure 5b). As the gap further diminishes, overlap of hot spot and molecule increases again, up to a point when the molecule can no longer fit inside (gap of *ca.* 15 nm).

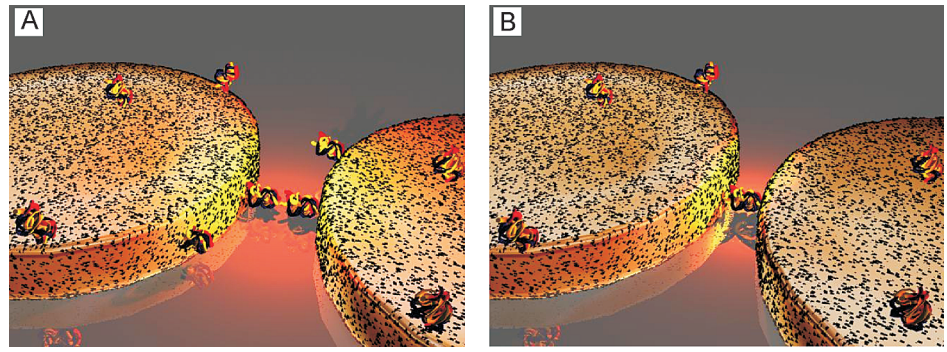

Figure 5. BSA binding in the gap of a gold dimer (a) when the gap size facilitates 2 molecules or (b) just a single molecule.

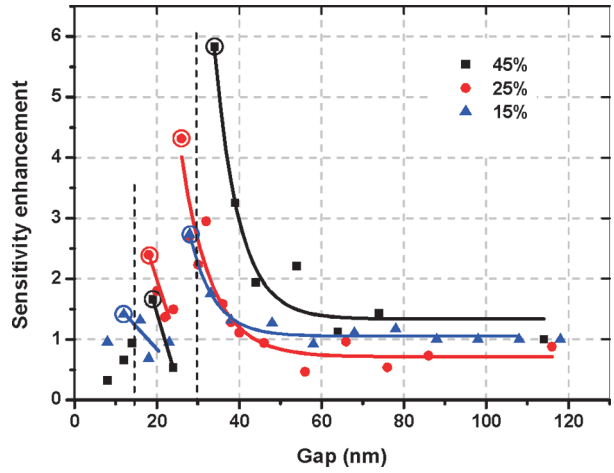

Figure 6. Evolution with the gap size of the sensitivity enhancement due to BSA binding: the enhancement is defined as the resonance shift normalized to the shift for isolated particles. Three different levels of MUA monolayer coverage are shown (45, 25, and 15%). Lines are partial exponential fit and used as a guide to the eye.

This interpretation may look simplified considering BSA is not a spherical molecule and that binding orientation inside the gap could vary. However, it is known that binding of BSA to glass substrates at the protein's isoelectric point favors a long axis linking and therefore suggests that BSA will protrude perpendicularly out from the surface.[33,34] Although this system is not glass, the protein could behave in an analogous fashion under similar binding conditions and thus on average extend from the surface. Additionally, this effect is reproducible, and strikingly, it has been found repeatedly within 4 nm around this critical 30 nm gap distance. The second drop, although less pronounced, occurs at 15 ± 2 nm, corroborating the hypothesis of specific BSA binding orientation. After the second drop, we observed smaller BSA-induced shifts than for the isolated MN case (Figure 4), as a consequence of reduced mode extension away from the gap and the inability of the BSA molecules to now penetrate into this area due to size exclusion.[29]

At this stage, it is hard to provide a reliable value for the limit of detection of our system. While there exists an analytical model to assess the sensitivity of SPR sensors based on extended metal films, its reliability for LSPR sensors is restricted to unpolarized illumination and/or symmetric shapes and arrangements of MNs.[24,30] In the case of dimers (strongly polarized illumination and asymmetric particle arrangement), it becomes a very poor approximation. Nevertheless, it is clear from our data that the limit of detection of plasmonic dimers is several times lower than with isolated MNs. In order to quantify this enhancement, we plot in Figure 6 the evolution of the BSA-induced shifts normalized to the shift of isolated MNs as a function of gap size. Three sets of results are presented corresponding to different MUA monolayer coverage varying between *ca.* 15 and 45%. For 45% coverage, a sensitivity enhancement of 6 is measured for a 34 nm gap. While we observed very reproducible dependences with the gap size for all three samples, we also confirmed that lower enhancements were obtained when decreasing MUA coverage. Conversely, this tends to indicate that more BSA binding sites should be available for complete monolayer formation, further inducing higher sensitivity (induced shift for the same analyte concentration). Thus, metallic nanoparticle dimer systems, combined with state-of-the-art single-particle dark field spectroscopy, could be good candidates to perform single-molecule sensing. Furthermore, simulations would help to reveal the actual sensing volume profile of the dimer system as a

function of gap size. They could make known what is the contribution of the molecules bound in the "cold regions" of dimers to the overall shift and help in the optimization of the sensing process regarding particular molecules of interest.

CONCLUSIONS

We have developed a fabrication procedure, using EBL on negative resist combined with RIE, to increase the control over the critical features of plasmonic dimers. By efficiently squeezing the sensing volume into truly nanovolumes, the detection sensitivity of biological proteins is shown to be increased by several times compared to isolated MNs. The same principle stands for more sensitive shapes (nanorods[31] nanoprisms[32]) as well as for different materials (silver). The initial drawback of whether the sensitivity of LSPR sensing could match that of conventional extended film SPR could now become a distinct reality through careful engineering of the MNs' shape, size, and distribution. Moreover, the work presented here, in turn, improves upon existing detectability and opens the way for low molecular weight analyte detection, without the need for labels, a particular sticking point for biosensor detection systems to date.

EXPERIMENTAL SECTION

Fabrication of Metal Nanoparticle Dimers. These were fabricated employing a novel fabrication process based on negative resist electron-beam lithography. Glass substrates were cleaned by ultrasound exposure in consecutive solutions for a period of 5 min each (detergent/deionized water (DIW) mixture, DIW, acetone, and finally ethanol). Thereafter, gold is thermally evaporated in high vacuum onto the cleaned substrate to a thickness of 40 nm, which determines the height of our particles. Negative resist (AR-N 7500.08, Alresist, Germany) was spun coated onto the gold layer, yielding a resist thickness of *ca.* 60 nm, as per manufacturer guidelines. A pre-exposure bake is done at 85 °C in a convection oven for 30 min. Electron-beam exposure was performed with a FEI Quanta 200 scanning electron microscope modified with Raith Elphy Plus lithography add-on, at a maximum voltage of 30 kV. After exposure, samples were developed in an AR 300-47 developer and DIW mixture (4:1) for a few minutes. The formation of masking nanostructures was confirmed by an optical microscope, followed by pre-etching resist baking in the oven for 1 h at 130 °C. Desired nanopatterns are transferred to the underlying gold layer by reactive ion etching (PlasmaLab 100, Oxford Instruments). Unprotected gold layer was removed in argon plasma by directional Ar ion bombardment. After removing unprotected gold, the remaining mask was etched away by isotropic etching in mild oxygen plasma.

Optical Characterization. Optical setup for measuring extinction response of MNs consisted of a standard microscope in bright field configuration: white light source (halogen 100 W), bright field condenser (0.1 NA), BF objective (10×, 0.25 NA). Light transmitted through the sample is collected by an objective and passed through a beam splitter into a CCD camera for alignment and to a spectrometer (Andor, Shamrock) *via* an optical fiber. Linear polarizer is placed before the BF condenser to provide linearly polarized light excitation.

Sensor Preparation. As part of the experimental procedure, each fabricated sample is first kept in ethanol for 24 h to allow for solvent annealing of the structures. Subsequently, the gold surface is functionalized with varying amounts of mercaptoundecanoic acid (MUA) by immersing the sample into MUA/ethanol solution for a further 24 h. Washing is accomplished by rinsing in ethanol after each of these steps. To bind strongly the protein of choice to the MUA monolayer, we first activate the acid of MUA by immersing the sample in a solution of EDC (20 mM) and NHS (5 mM) in 0.1 M MES, pH 4.7 for 30 min and bind bovine serum albumin (BSA) through its lysine moiety, again by immersing the sample to a solution of 50 μg/mL BSA (50 mM PBS, pH 5) for 90 min. Washing in these latter steps occurs by rinsing in PBS and DIW. After each step of the binding process, samples are carefully blown dry in a stream of nitrogen and optically characterized for their corresponding resonance shifts (as outlined above).

Acknowledgment. This research has been funded by the Spanish Ministry of Sciences through Grant Nos. TEC2007-60186/MIC and CSD2007-046-NanoLight.es and by the CELLEX Foundation. M.K. and M.G. acknowledge support from the Ramon y Cajal program.

REFERENCES AND NOTES

1. De Angelis, F.; Patrini, M.; Das, G.; Maksymov, I.; Galli, M.; Businaro, L.; Andreani, L. C.; Di Fabrizio, E. A Hybrid Plasmonic-Photonic Nanodevice for Label-Free Detection of a Few Molecules. *Nano Lett.* **2008**, *8*, 2321–2327.
2. Sannomiya, T.; Hafner, C.; Voros, J. *In Situ* Sensing of Single Binding Events by Localized Surface Plasmon Resonance. *Nano Lett.* **2008**, *8*, 3450–3455.
3. Willets, K. A.; Van Duyne, R. P. Localized Surface Plasmon Resonance Spectroscopy and Sensing. *Annu. Rev. Phys. Chem.* **2007**, *58*, 267–297.
4. Anker, J. N.; Hall, W. P.; Lyandres, O.; Shan, N. C.; Zhao, J.; Van Duyne, R. P. Biosensing with Plasmonic Nanosensors. *Nat. Mater.* **2008**, *7*, 442–453.
5. Nie, S.; Emory, S. R. Probing Single Molecules and Single Nanoparticles by Surface-Enhanced Raman Scattering. *Science* **1997**, *275*, 1102–1106.
6. Kneipp, K.; Yang Wang, Y.; Kneipp, H.; Perelman, L. T.; Itzkan, I.; Dasari, R. R.; Feld, M. S. Single Molecule Detection Using Surface-Enhanced Raman Scattering (SERS). *Phys. Rev. Lett.* **1997**, *78*, 1667–1670.
7. Larsson, E. M.; Alegret, J.; Kall, M.; Sutherland, D. S. Sensing Characteristics of NIR Localized Surface Plasmon Resonances in Gold Nanorings for Application as Ultrasensitive Biosensors. *Nano Lett.* **2007**, *7*, 1256–1263.
8. Haes, J.; Haynes, C. L.; Van Duyne, R. P. Nanosphere Lithography: Self-Assembled Photonic and Magnetic Materials. *Mater. Res. Soc. Symp. Proc.* **2001**, *636*, D4.8.
9. Kravets, V. G.; Schedin, F.; Grigorenko, A. N. Extremely Narrow Plasmon Resonances Based on Diffraction Coupling of Localized Plasmons in Arrays of Metallic Nanoparticles. *Phys. Rev. Lett.* **2008**, *101*, 087403.
10. Auguie, B.; Barnes, W. L. Collective Resonances in Gold Nanoparticle Arrays. *Phys. Rev. Lett.* **2008**, *101*, 143902.
11. Xu, H.; Aizpurua, J.; Kall, M.; Apell, P. Electromagnetic Contributions to Single-Molecule Sensitivity in Surface-Enhanced Raman Scattering. *Phys. Rev. E* **2000**, *62*, 4318–4324.
12. Kottmann, J. P.; Martin, O. J. F. Plasmon Resonant Coupling in Metallic Nanowires. *Opt. Exp.* **2001**, *8*, 655–663.
13. Romero, I.; Aizpurua, J.; Bryant, G. W.; Garcia de Abajo, F. J. Plasmons in Nearly Touching Metallic Nanoparticles: Singular Response in the Limit of Touching Dimers. *Opt. Exp.* **2006**, *14*, 9988–9999.
14. Ghenuche, P.; Cherukulappurath, S.; Taminiau, T. H.; Van Hulst, N. F.; Quidant, R. Spectroscopic Mode Mapping of Resonant Plasmon Nanoantennas. *Phys. Rev. Lett.* **2008**, *101*, 116805.

15. Imura, K.; Okamoto, H.; Hossain, M. K.; Kitajima, M. Visualization of Localized Intense Optical Fields in Single Gold-Nanoparticle Assemblies and Ultrasensitive Raman Active Sites. *Nano Lett.* **2006**, *6*, 2173–2176.
16. Enoch, S.; Quidant, R.; Badenes, G. Optical Sensing Based on Plasmon Coupling in Nanoparticle Arrays. *Opt. Exp.* **2004**, *12*, 3422–3427.
17. Jain, P. K.; El-Sayed, M. A. Noble Metal Nanoparticle Pairs: Effect of Medium for Enhanced Nanosensing. *Nano Lett.* **2008**, *8*, 4347–4352.
18. Kreuzer, M. P.; Quidant, R.; Badenes, G.; Marco, M. P. Quantitative Detection of Doping Substances by a Localised Surface Plasmon Sensor. *Biosens. Bioelectron* **2006**, *21*, 1345–1349.
19. Haes, A. J.; Chang, L.; Klein, W. L.; Van Duyne, R. P. Detection of a Biomarker for Alzheimer's Disease from Synthetic and Clinical Samples Using a Nanoscale Optical Biosensor. *J. Am. Chem. Soc.* **2005**, *127*, 2264–2271.
20. Riboh, J. C.; Haes, A. J.; McFarland, A. D.; Ranjit Yonzon, C.; Van Duyne, R. P. A Nanoscale Optical Biosensor: Real-Time Immunoassay in Physiological Buffer Enabled by Improved Nanoparticle Adhesion. *J. Phys. Chem. B* **2003**, *107*, 1772–1780.
21. McFarland, A. D.; Van Duyne, R. P. Single Silver Nanoparticles as Real-Time Optical Sensors with Zeptomole Sensitivity. *Nano Lett.* **2003**, *3*, 1057–1062.
22. Atay, T.; Song, J. H.; Nurmikko, A. V. Strongly Interacting Plasmon Nanoparticle Pairs: From Dipole−Dipole Interaction to Conductively Coupled Regime. *Nano Lett.* **2004**, *4*, 1627–1631.
23. Jain, P. K.; Huang, W.; El-Sayed, M. A. On the Universal Scaling Behaviour of the Distance Decay of Plasmon Coupling in Metal Nanoparticle Pairs: A Plasmon Ruler Equation. *Nano Lett.* **2007**, *7*, 2080–2088.
24. Su, K. H.; We, Q. H.; Zhang, X.; Mock, J. J.; Smith, P. R.; Schultz, S. Interparticle Coupling Effects on Plasmon Resonances of Nanogold Particles. *Nano Lett.* **2003**, *3*, 1087–1090.
25. Reinhard, B. M.; Siu, M.; Agarwal, H.; Alivisatos, A. P.; Liphardt, J. Calibration of Dynamic Molecular Rulers Based on Plasmon Coupling Between Gold Nanoparticles. *Nano Lett.* **2005**, *5*, 2246–2252.
26. Malinsky, M. D.; Kelly, K. L.; Schatz, G. C.; Van Duyne, R. P. Chain Length Dependence and Sensing Capabilities of the Localized Surface Plasmon Resonance of Silver Nanoparticles Chemically Modified with Alkanethiol Self-Assembled Monolayers. *J. Am. Chem. Soc.* **2001**, *123*, 1471–1482.
27. Grigorenko, A. N.; Gleeson, H. F.; Zhang, Y.; Roberts, N. W.; Sidorov, A. R.; Panteleev, A. A. Antisymmetric Plasmon Resonance in Coupled Gold Nanoparticles as a Sensitive Tool for Detection of Local Index of Refraction. *Appl. Phys. Lett.* **2006**, *88*, 124103.
28. Barbillon, G.; Bijeon, J. L.; Plain, J.; Lamy de la Chapelle, M.; Adam, P. M.; Royer, P. Electron Beam Lithography Designed Chemical Nanosensors Based on Localized Surface Plasmon Resonance. *Surf. Sci.* **2007**, *601*, 5057–5061.
29. Ringler, M.; Klar, T. A.; Schwemer, A.; Susha, A. S.; Stehr, J.; Raschke, G.; Funk, S.; Borowski, M.; Nichtl, A.; Kruzinger, K.; Phillips, R. T.; Feldmann, J. Moving Nanoparticles with Raman Scattering. *Nano Lett.* **2007**, *7*, 2753–2757.
30. Rechberger, W.; Hohenau, A.; Leitner, A.; Krenn, J. R.; Lamprecht, B.; Aussenegg, F. R. Optical Properties of Two Interacting Gold Nanoparticles. *Opt. Commun.* **2003**, *220*, 137–141.
31. Aizpurua, J.; Bryant, G. W.; Richter, L. J.; Garcia de Abajo, F. Optical Properties of Coupled Metallic Nanorods for Field-Enhanced Spectroscopy. *Phys. Rev. B* **2005**, *71*, 235420.
32. Fromm, D. P.; Sundaramurthy, A.; Schuck, P. J.; Kino, G.; Moerner, W. E. Gap-Dependent Optical Coupling of Single Bowtie Nanoantenas Resonant in the Visible. *Nano Lett.* **2004**, *4*, 957–961.
33. Fitzpatrick, H.; Luckham, P. F.; Eriksen, S.; Hammond, K. Bovine Serum Albumin Adsorption to Mica Surfaces. *Colloids Surf.* **1992**, *65*, 43–49.
34. Su, T. J.; Lu, J. R.; Thomas, R. K.; Cui, Z. F. Effect of pH on the Adsorption of Bovine Serum Albumin at the Silica/Water Interface Studied by Neutron Reflection. *J. Phys. Chem. B* **1999**, *103*, 3727–3736.